Jurnal Teknologi

Full Paper

PRODUCTION OF CELLULOSE NANOCRYSTALS FROM OIL PALM EMPTY FRUIT BUNCH AND PINEAPPLE LEAF FIBRE USING DOUBLE OXIDATION APPROACH

Raimi Fariz Nasrudin[a], Noorasikin Samat[a*], Nur Afiqah Mokhtar[a], Norzita Yacob[b]

[a]Department of Manufacturing and Materials Engineering, IIUM, Jalan Gombak, 53100, Gombak, Kuala Lumpur, Malaysia
[b]Radiation Processing Technology Division, Malaysia Nuclear Agency, 43000, Kajang, Selangor, Malaysia

Article history
Received
18 January 2022
Received in revised form
8 June 2022
Accepted
19 June 2022
Published Online
21 August 2022

*Corresponding author
noorasikin@iium.edu.my

Graphical abstract

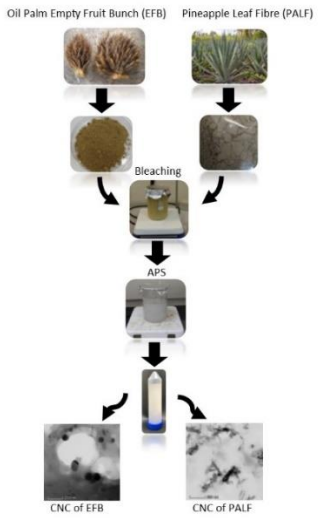

Abstract

Cellulose nanocrystasl (CNC) were produced from oil palm empty fruit bunch (EFB) and pineapple leaf fibre (PALF) using double oxidation treatment comprising bleaching and ammonium persulfate (APS) treatments. Different techniques were used to characterise the extracted CNC. Fourier transform infrared (FTIR) spectra confirmed the formation of carboxyl group and decreasing fractions of non-cellulosic components. The CNCs from both fibres show a better crystallinity index than the raw fibre, and the CNCs also conform to the crystalline structure of cellulose I. Morphology analysis using transmission electron microscopy (TEM) reveals that the CNCs of EFB and PALF have different shapes and dimensions. Spherical EFB had a 16.33 ± 8.5 nm diameter, while rod-like PALF had 13.07 ± 6.15 nm and 78.67 ± 38.07 nm diameter and length. However, the thermal stability of both CNCs decreased slightly. Hence, the findings indicate that the double oxidation approach using agricultural biomass wastes can work as an alternative route for the preparation of CNCs.

Keywords: Nanocellulose, ammonium persulfate oxidation, bleaching, crystallinity index, thermal stability

Abstrak

Nanokristal selulosa (CNC) diperoleh daripada tandan kosong kelapa sawit (EFB) dan serat daun nanas (PALF) menggunakan rawatan pengoksidaan berganda yang terdiri daripada rawatan pelunturan dan ammonium persulfat (APS). Pelbagai teknik yang berbeza digunakan untuk mencirikan CNC yang diekstrak. Spektrum inframerah transformasi Fourier (FTIR), mengesahkan pembentukan kumpulan karboksilik bersama-sama dengan pecahan komponen bukan selulosa yang semakin berkurang. CNC bagi kedua-dua gentian menunjukkan indeks kehabluran yang lebih baik berbanding dengan gentian mentah, dan CNC juga mematuhi struktur kristal selulosa I. Analisis morfologi daripada TEM mendedahkan bahawa CNC EFB dan PALF mempunyai bentuk dan dimensi yang berbeza. Diameter EFB sfera adalah kira-kira 16.33 ± 8.5 nm, manakala diameter dan panjang PALF seperti rod adalah sekitar 13.07 ± 6.15 nm dan 78.67 ± 38.07 nm, masing-masing. Walau bagaimanapun, sifat kestabilan haba kedua-dua CNC berkurangan sedikit. Oleh itu, penemuan ini menunjukkan bahawa pendekatan pengoksidaan berganda menggunakan sisa biojisim pertanian boleh berfungsi sebagai kaedah alternatif untuk penyediaan CNC.

Kata kunci: Nanokristal selulose, pengoksidaan ammonium persulfate, pelunturan, indeks kehabluran, kestabilan haba

© 2022 Penerbit UTM Press. All rights reserved

1.0 INTRODUCTION

Cellulose is a class of natural carbohydrate polymer widely available in various plants, animals and bacteria. Hence, it is renewable and biodegradable. Annually, 75–100 billion tonnes of cellulose are produced across the globe [1-2]. Generally, the main constituents in the cell wall of any plant fibre are cellulose, hemicellulose, and lignin. Cellulose exists in fibrous form as a result of the β-1, 4-glycosidic linkages that combine the glucose monomers. The production or extraction of cellulose by removing amorphous counterparts produces nano-structured cellulose called nanocellulose. It possesses unique physical, chemical, and mechanical properties such as low density, large specific surface area, high crystallinity, and tensile strength. These properties make cellulose and nanocellulose a choice material for various applications, including water remediation [3-4], energy storage [5], biomedical products [6], composite matrix reinforcement for [7-8] and hybrid materials in aerogels and hydrogels [9]. Cellulose has another distinctive feature; it can be retrieved from numerous abundant natural sources. Nanocellulose extraction from agricultural residue creates value for such waste and helps reduce waste disposal-based environmental problems. Empty fruit bunch (EFB) and pineapple leaf fibre (PALF) are biomass wastes produced from palm oil fruit and pineapple tree. This waste has attracted researcher's attention because palm oil and pineapple trees are planted in many developing countries [10-11]. The massive availability of EFB and PALF and their cellulose content make them a promising feedstock to produce cellulose and nanocellulose.

Based on its morphology, nanocellulose can be classified into cellulose nanofibril (CNF) and cellulose nanocrystal (CNC). Generally, CNF has a 5–60 nm diameter and micron-scale length [12]. However, CNCs are rod-like structures having 5–20 nm and 100–300 nm diameter and length [13–15]. Specific chemicals are used to functionalise CNC to suit several applications. Through the chemical treatment, negative or positive electrostatic charges are established on the CNC surfaces. CNC is more advantageous than CNF because the former has higher crystallinity; moreover, CNC-incorporated polymer films have better transparency than CNF films [16].

CNC can be obtained using a primary production technique called acid hydrolysis. After the treatment, the presence of charged sulfate enables the produced CNC to disperse readily in water [17-18]; however, it reduces thermal stability, ultimately limiting CNC applications [19]. The oxidation treatment approach has been acknowledged to generate the carboxyl group on CNC surfaces. The anionic charge of the carboxyl group is also responsible for the electrostatic repulsion of carboxylated CNC [14, 20].

During oxidation treatment, the hydroxyl group of the glucose unit changes into a carbonyl group at C6 points (-C^6H_2OH ➔-C^6OOH) [21]. 2,2,6,6-tetramethylpiperidine-1-oxyl (TEMPO)-mediated oxidation is extensively used for oxidation. However, TEMPO-oxidised fibre needs to be treated further via acid hydrolysis [22] or mechanical treatments [13]. Ammonium persulfate (APS) is also used in the oxidation process to obtain the CNC. Compared to TEMPO-oxidation, APS treatment is relatively straightforward than TEMPO-oxidation and has minimal long-term toxicity. Treatment is usually takes longer times despite procedural simplicity. Several studies on CNC extraction from natural fibres indicate that 1M APS, treatment requires 16 hours [21, 23–26]. Furthermore, APS treatment has oxidation efficiency limitations concerning various biomass wastes. For instance, a 16-hour direct APS oxidation of an empty fruit bunch (EFB) only produces microfibrillated cellulose (MFC) and not CNC [27].

Many articles focus primarily on obtaining CNC by comparing it with other typical production methods (APS with acid hydrolysis or TEMPO-oxidation) [24, 28] or varying the treatment parameters like heating temperature, APS concentration, and oxidation time [14, 18, 25]. Little research has been done on coupling the APS oxidation treatment with other methods. Filipova *et al*. [28] combined the APS treatment with ultrasonic and mechanical processing for treating the bleached birch Kraft pulp fibres to obtain CNF. Meanwhile, Du *et al*. and the team [29] produced rod-like CNCs from bleached bagasse pulp treated with APS solution. Before performing APS oxidation treatment, both works used bleached fibre as the starting material.

Hence, this study aims to investigate the effects of double oxidation treatments comprising bleaching and APS for CNC extraction. The CNC was obtained from two sources of agricultural residue: EFB and PALF. The morphology, functional groups, crystallinity, and thermal stability properties of isolated CNC were compared using scanning electron microscopy (SEM), transmission electron microscopy (TEM), Fourier transform infrared spectroscopy (FTIR), X-ray diffraction (XRD), and thermogravimetric analysis (TGA). The characterisation results were also compared with a direct 16-hrs APS treatment.

2.0 METHODOLOGY

2.1 Materials

Two locally-obtained biomass types were used as the raw materials: EFB and PALF. The Malaysia Palm Oil Board (MPOB), Bangi, Selangor, provided the EFB, while a local plantation owner in Sungai Merab Luar, Kajang, Selangor, provided the PALF. Sodium chlorite ($NaClO_2$) was purchased from Morning Prestige Trading. Fischer Scientific Sdn Bhd supplied other chemicals such as the APS, acetic acid, and sulphuric acid were supplied by. The fibres were dried, crushed, blended, and sieved using a 45 µm mesh.

2.2 $NaClO_2$ Bleaching and APS Oxidation

First, $NaClO_2$ solution 0.7% (w/v) was prepared, and acetic acid was added to acidify the solution to

achieve a pH value of 4. Then, the fibres were heated in the $NaClO_2$ solution for 2 hrs at 70 °C. The bleaching process was repeated several times until the suspension turned white. The suspension was then centrifuged for 10 min at 5000 rpm. This process was repeated until the suspension reached a pH value of 4, after which it was air-dried. Next, the bleached fibre was treated with the APS solution.

1 M APS was prepared by diluting the APS in distilled water. Then, 1 g of the fibre was mixed with the APS solution at 85 °C and stirred mechanically using a magnetic stirrer for 9 hrs. The 9-hr oxidation time was determined based on our previous unpublished works. The oxidised fibres were centrifuged for 10 minutes at 5000 rpm and washed until the pH value reached 4. Next, the fibre were subjected to sonication in an ice bath (Branson 1510, Ultrasonic sonicator water bath) for 30 min. Subsequently, the dispersed fibres were lyophilised or freeze-dried for 4 days. The dried samples were stored in a dry cabinet for further use. Table 1 summarises fibre notations and treatment. CNC yield percentage was determined using the final and initial fiber weight.

Table 1 Notation of EFB and PALF samples

Samples	Bleaching	APS oxidation
E-EFB	-	-
B-EFB	√	-
A-EFB9	√	√
A-EFB16	√	√
R-PALF	-	-
B-PALF	√	-
A-PALF9	√	√
A-PALF16	√	√

2.3 Characterization

The functional groups or chemical structures of both untreated and treated cellulose samples were investigated using an FTIR spectrometer (Invenio, Bruker). The machine was operated within the 4000 – 400 cm^{-1} range, using a resolution of 4 cm^{-1}. The degree of oxidation (DO) is calculated from the FTIR spectra based on Equation 1 [23]:

$$DO = 0.01 + 0.7(I_{CO} / I_{COC}) \quad (1)$$

where I_{CO} is the carbonyl peak near 1733 cm^{-1}, and I_{COC} refers to the highest peak close to 1060 cm^{-1}.

The crystallinity of the celluloses was analysed using an X-ray diffractometer (D2 Phaser, Bruker), where the copper K-alpha (Cu K-a) x-rays were operated at 40 kV and 40 mA current. The cellulose was scanned from 5° to 50° (2θ) using a 0.02° step mode with a scan rate of 37 s/step. The crystallinity index (CrI) is calculated using Equation 2:

$$CrI\ (\%) = (I_{200} - I_{am}) / I_{200} \times 100 \quad (2)$$

where CrI represents the crystallinity index (%), I_{200} is the maximum intensity of the peak at 2θ = 22.5°. Meanwhile, I_{am} is the amorphous peak intensity taken at an angle of 2θ = 18.6° in the valley between the peaks.

The morphologies of APS treated EFB and PALF were observed using a scanning electron microscope (SEM; JSM 5600) operating at 7 kV, and a transmission electron microscope (TEM) (H7650 Hitachi Ltd. Japan) operating at 200 kV. The samples were coated with palladium using an auto fine-coater (Quorum Tech. SC7620 Mini Sputter Coater). Before the TEM characterisation, the nanocellulose suspension (0.01%) was stained with a 3.0 wt% phosphotungstic acid solution for 2 min and dried at room temperature. CNC dimensions were measured using digital image analysis (ImageJ software). A thermogravimetric analyser (STA 7300, Hitachi) was used to study the thermal stability of the samples. A small amount of fibre was placed in a platinum pan and heated to 1000 °C at a rate of 10 °C/min. The heating chamber was supplied with a low argon gas flow at 100 mL/min.

3.0 RESULTS AND DISCUSSION

3.1 Chemical Composition Analysis

FTIR analysis was conducted to evaluate the change in the chemical structures of EFB and PALF fibres before and after bleaching and APS treatments. Figure 1 shows that the FTIR spectra of R-EFB, R-PALF and CNCs (A-EFB9 and A-PALF9) have quite similar absorption peaks with minor wavelength shifts. For absorption wavelength beyond 2000 cm^{-1} (left side), all samples (untreated and treated) exhibit the typical cellulose absorption peak characteristics. It is suggested that the primary chemical structure of cellulose was not affected by bleaching and APS treatments. The primary absorbance bands of cellulose molecules for raw fibre, bleached fibre and CNC were seen at 3337–3335 cm^{-1} and 2892–2895 cm^{-1}. These peaks corresponded to the stretching vibrations corresponding to hydrogen bonds in the O–H and C–H groups, respectively.

However, concerning absorption wavelength below 2000 cm^{-1} (towards the right), the first absorption peak between 1733–1728 cm^{-1} indicates lignin and hemicellulose. These peaks relate to the C=O stretching at acetyl and uronic ester groups of the hemicelluloses and the ester linkage of carboxylic groups of the ferulic and lignin's p-coumaric acids. Despite a slight decrease in the absorption intensity of the bleached fibre, the A-EFB9 and A-PALF9 or CNC samples retained the corresponding absorption peaks. This peak in the CNC samples indicates the success of carboxylation onto the surface of CNC after APS oxidation treatment. Like many previous works, the interaction between water and cellulose related to the O–H bending of absorbed water was indicated at peaks between 1640-1642 cm^{-1} [30-31].

The presence of lignin and hemicellulose in raw EFB and PALF is also evident at 1510 cm^{-1} and 1246 cm^{-1}, respectively. A small peak at 1510 cm^{-1} corresponds to

the C=C vibration in the aromatic skeleton of lignin. The vibration of –COO of acetyl group of hemicellulose was prominent at 1246 cm^{-1} [32]. The absorption peak at 1510 cm^{-1} disappeared almost entirely for the bleached fibre, while there was reduced intensity for the absorption peak at 1246 cm^{-1}. The absorption peak changes imply that most lignin and partial hemicellulose in the raw EFB and PALF were removed due to bleaching. In this work, the raw fibre was treated directly without alkali pre-treatment. Indeed, the absence of pre-treatment did not affect the efficiency producing the nanocellulose in both fibre types. This result aligns with the work by Ching and Ng [33].

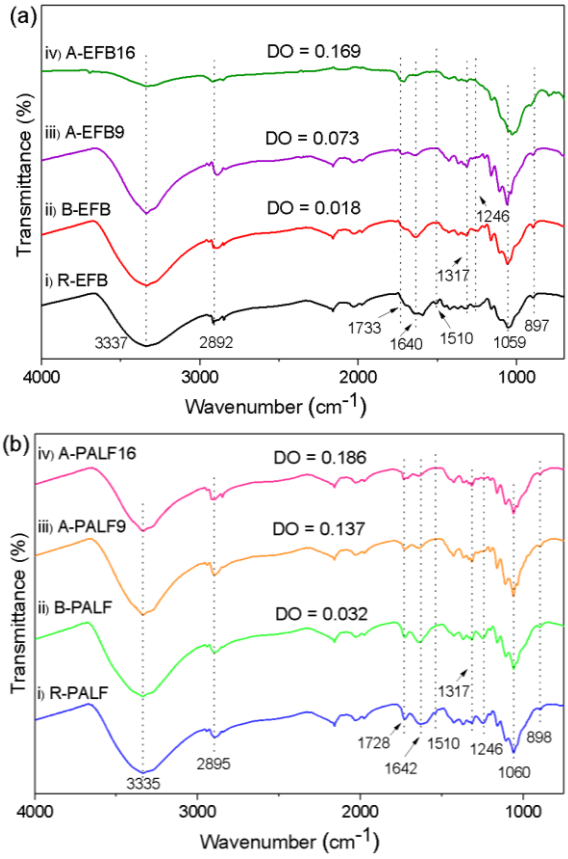

Figure 1 FTIR spectra of (a) EFB fibres and (b) PALF fibres

This observation suggests that bleaching treatment alone could not completely eliminate the non-cellulosic components. Hence, further treatment with APS oxidation would promote the degradation of residual lignin and hemicellulose, and eventually lead to the defibrillation or production of CNC. As a result, peaks at 1510 cm^{-1} and 1246 cm^{-1} disappeared in A-EFB9 and A-PALF9 samples. For the direct 16-hr APS oxidation treatment, the non-cellulosic peaks (1510 cm^{-1} and 1246 cm^{-1}) were absent in its IR spectra (Figure 1). Hence, it is clear that the bleaching and 9-hr APS treatment can sufficiently degrade non-cellulosic components, similar to the case of direct 16-hr-APS oxidation treatment.

At the lower absorption wavelength range (below 1500 cm^{-1}), all IR spectra show peaks at 1317 cm^{-1}, corresponding to the in-plane bending vibration of H–C–H and O–C–H. The prominent peak between 1059-1060 cm^{-1} was attributed to the C-O-C bending. These intensity peaks were higher after the APS treatment, indicating higher non-cellulosic part degradation, enhancing crystalline cellulose content as indicated in XRD analysis (Figure 2). The glucose units in cellulose are joined via the β (1−4) glycosidic linkage and the presence of this linkage is evident at 897 cm^{-1} [18]. The number of carbonyl groups introduced after the APS treatment was estimated from the FTIR spectrum using Equation 1 [25] and the calculated DO is given in Figure 1. Regardless of treatment types, the DO value of A-PALF was more prominent than that of A-EFB. The DO values also increased with the increase in oxidation time (16 hrs).

3.2 Crystallinity Analysis

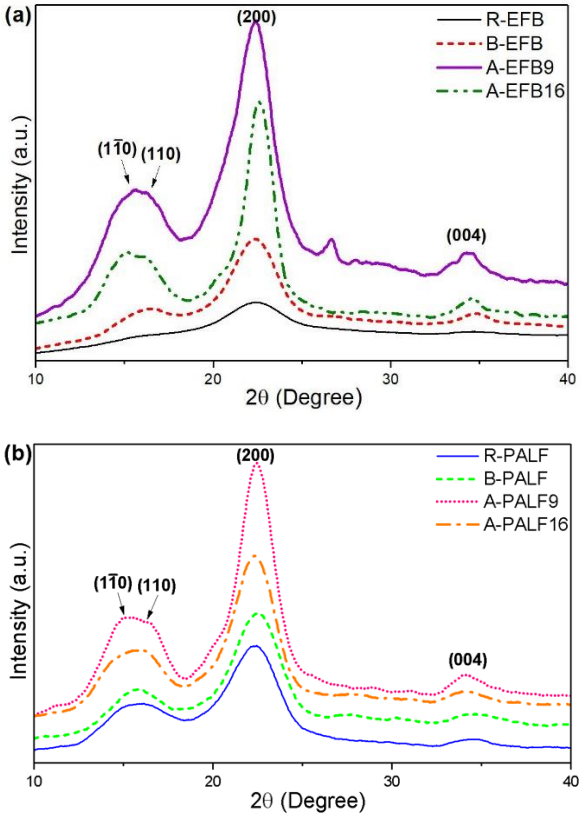

Figure 2 XRD diffractograms for (a) EFB and (b) PALF samples with different treatments fibres

The XRD patterns for all samples are depicted in Figure 2. XRD was used to compare the post-oxidation crystallinity of EFB and PALF. All samples exhibit several diffraction peaks, which were indexed as cellulose I at 2θ = 14.7° − 16°, 22° − 23° and 34.7° [34] for planes (1$\bar{1}$0), (110), (200) and (004), respectively. The diffraction peak patterns of EFB, PALF and their CNCs did not differ significantly. The change occurred in the diffraction

peak intensity and peak characteristic. As observed in Figure 2, the peak intensity increased, while the broad peak at 2θ = 14.7° − 16°, which corresponds to planes (1$\bar{1}$0) and (110), left-tilted slightly [20]. These changes were progressively occurred from the applied fibre treatments. Indeed, this observation further suggests that both fibres' crystal structure did not deteriorate during cellulose extraction. In this work, the CrI percentage was calculated and compared. The values are summarised in Table 2.

Table 2 Crystallinity index (CrI) of EFB and PALF fibres

Samples	2θ(°) = 200	2θ(°) = am	CrI (%)
R-EFB	22.40	18.30	28.40
B-EFB	22.35	18.19	37.10
A-EFB9	22.37	18.36	73.80
A-EFB16	22.56	18.48	69.80
R-PALF	22.40	18.30	43.27
B-PALF	22.54	18.28	48.67
A-PALF9	22.41	18.26	68.58
A-PALF16	22.25	18.41	66.75

**am = amorphous*

Table 2 shows that the CrI values of raw EFB and PALF increased from 28.4% and 43.27% to 37.1% and 48.67%, respectively. Both fibres had a CrI increase of less than 30%, indicating that the fraction of amorphous components still exists. Apparently, the subsequent treatment of bleached fibre with APS oxidation affects the CrI values more significantly in EFB. The CrI percentage was increased to 73.8% and 68.6% for EFB and PALF, respectively. CrI changes associated with the applied treatment provide further evidence concerning the removal of non-cellulosic components, which aligns with the FTIR analysis. Table 2 also shows that the CrI values decreased when oxidation time was increased to 16 hrs. Presumably, the degradation also took place in the cellulosic parts.

3.3 Morphological Analysis

Figure 3 shows the morphology of EFB and PALF characterised using SEM and TEM. Raw EFB (Figure 3a) and PALF (Figure 3b) exhibit a large fibre bundle of about 20 µm size. A rough fibre surface is attributed to the existence of cementing cellulose, non-cellulosic (hemicellulose and lignin) components, and impurities (wax, pectin, and oil). Fibre bleaching treatment efficiency is noticeable in Figures 3c-d. The fibre bundle had detached into micro-fibrils; the diameter had decreased to about ~5 µm. The fibrils surfaces were also seen smoother than the raw fibres, which confirmed the removal fractions of lignin, hemicellulose, and impurities from the raw fibres. This observation correlates well with the results discussed in the FTIR and XRD analyses.

The TEM micrographs (Figures 3e-g) reveal the transformation of bleached fibre from micro-fibril into CNC after the APS oxidation treatment. Figures 3e and 3g show that the EFB had a spherical shape with an average diameter of 16.33 ± 8.5 nm, while Figures 3f and 3h show that the PALF appears as a rod-like structure with a longitudinal dimension of 78.67 ± 38.07 nm and a width of approximately 13.07 ± 6.15 nm. Hence, these micrographs corroborated that double oxidation treatment (bleaching and 9-hr APS oxidation) is also effective in producing the CNC.

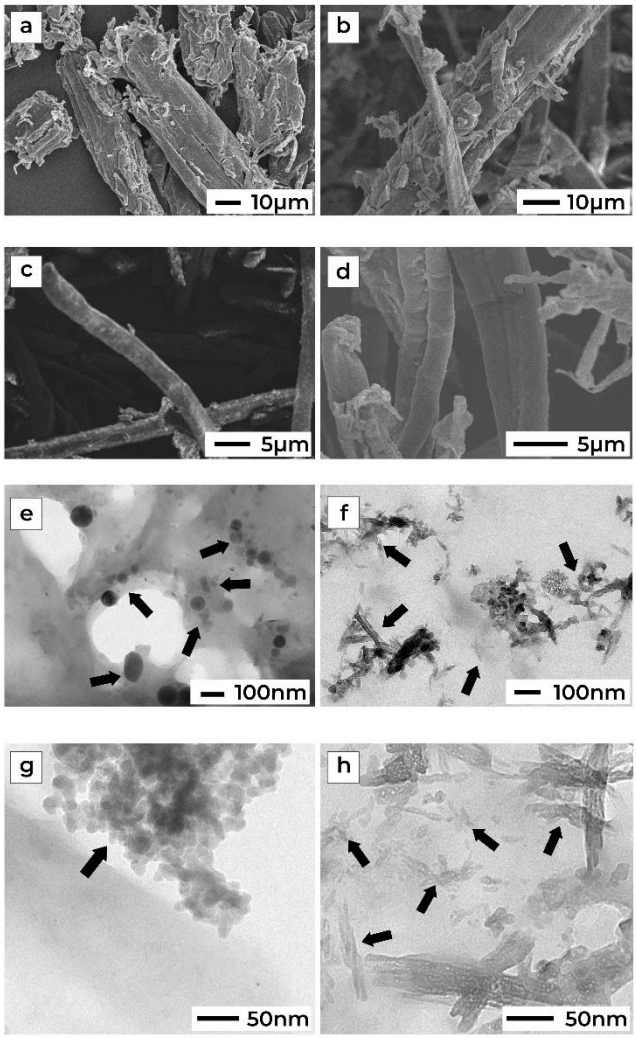

Figure 3 SEM micrograph of raw (a-b), bleached (c-d) and TEM micrographs of (e-h) of EFB and PALF samples, respectively

The CNCs of EFB and PALF produced in this work are consistent with other researchers' findings. As depicted in Table 3, a similar EFB nanocellulose morphology profile (spherical shape) was also reported by Azrina *et al.* [36]. However, in their work, acid hydrolysis was used together with ultrasound. Moreover, nanocellulose diameter was also slightly larger than that obtained in this study. Contrarily, studies on PALF nanocellulose extraction using the APS treatment were unavailable in the open literature. Various other extraction methods have been applied, and the morphology of acquired cellulose also differed. Rod-like structures did not form; however, nanofibril structures were discovered (Table 3).

Table 3 Comparison of morphology and dimensions of nanocellulose from EFB and PALF

Fiber	Morphology	Method	Reference
Borer powder of bamboo	1. Spherical shape CNC, D = 20-50 nm 2. Spherical shape CNC, D = 20-70 nm	1. APS 2)Acid Hydrolysis	Hu *et al.* [35]
EFB	Spherical shape CNC. D = 30 -40 nm	Ultrasound assisted acid hydrolysis process	Azrina *et al.* [36]
EFB	Rod-like shape CNC, D = 6.78 ± 2.12 nm, L = 160.06 ± 32.58 nm	Acid hydrolysis preceded by alkaline deep eutectic solvent (DES) pretreatment and bleaching	Gan *et al.* [19]
EFB	Rod-like shape CNC, D = 43 ± 8 nm, L = 147 ± 23 nm.	Alkaline and bleached ($NaClO_2$), then hydrolysed using sulfuric acid	Burhani and Septevani [37]
EFB	Spherical shape CNC, D = 16.33 ± 8.5 nm	Bleaching and APS	Current work
PALF	CNF, D = 22 ± 3 nm	Acid coupled steam explosion process	Deepa *et al.* [38]
PALF	CNF, D = 10 - 50 nm	Lime juice and ball milling	Ravindrana *et al*. [39]
PALF	CNF, D = 40–70 nm	Pretreatment (pulping, bleaching)and acid hydrolysis, followed by high-shear homogenization and ultrasonication	Mahardika *et al.* [40]
PALF	Rod-like shape CNC, D = 13.07 ± 6.15 nm, L = 78.67 ± 38.07 nm	Bleaching and APS	Current work

**D = diameter; L= length*

In the current study, similar chemical treatments and production conditions were exploited. However, different morphological and XRD results were obtained. Therefore, it can be emphasised that the extraction of nanocellulose is dominated by cellulose source, whereby it is associated with the high crystallinity index (CrI) value of raw PALF (Table 2). It is well accepted that the CrI parameter represents the relative amount of crystalline phase in the material. According to Hall *et al.* [41], highly crystalline materials have tighter structures. This phenomenon reduces the accessibility of chlorine dioxide from bleaching agent to react with crystalline PALF parts. In contrast, the amorphous parts are more susceptible to digestion through bleaching. Although bleaching is conducted to dissolve lignin, but hemicellulose and other impurities (wax, oil, etc.) might also be affected, as observed in the FTIR analysis. Consequently, the fibre bundle was separated into micro-fibril with smooth surfaces, which decreased the fibre diameter. Indeed, removing non-cellulosic components in PALF is considered minimal, as reflected by its lower CrI value than EFB. Bleaching based degradation occurred through acidic cleavage of the glycosidic bonds and oxidative degradation of polysaccharides [42]. Hence, this condition will promote the accessibility of APS oxidation to amorphous residue in the microfibrils. More inter-fibril hydrogen bonds would break, facilitating nanocellulose production. Since raw EFB has a lower CrI value, EFB had a greater APS-oxidation rate. Consequently, EFB exhibited spherical cellulose formation.

Both fibres exhibit different yield percentages. EFB CNC showed the lowest yield of 15.4% at 9 hrs. However, PALF fibre produced higher CNC yields of 29.6% (9 hrs). These results show that the type of initial source fibre significantly influence yield percentage.

3.4 Thermal Analysis

The effect of double oxidation treatment on fibres' thermal stability was measured with a thermogravimetric analyser, and the results are exhibited in Figure 4. A similar thermal decomposition curve pattern, namely, double mass loss steps, was observed for all samples. The initial weight loss of less than 5% for all samples was at a temperature below 100 ^{O}C. As reported in most previous works on lignocellulosic materials, the weight loss drop was attributed to moisture evaporation from the sample surface. The degradation onset temperature (T_{os}), maximum temperature (T_{max}), and the percentage of char residue were recorded, as in Table 4. R-PALF had a slightly better T_{os} than R-EFB due to a higher crystallinity percentage, as depicted in the XRD analysis. As expected, eliminating lignin and hemicellulose during bleaching treatment would improve thermal stability.

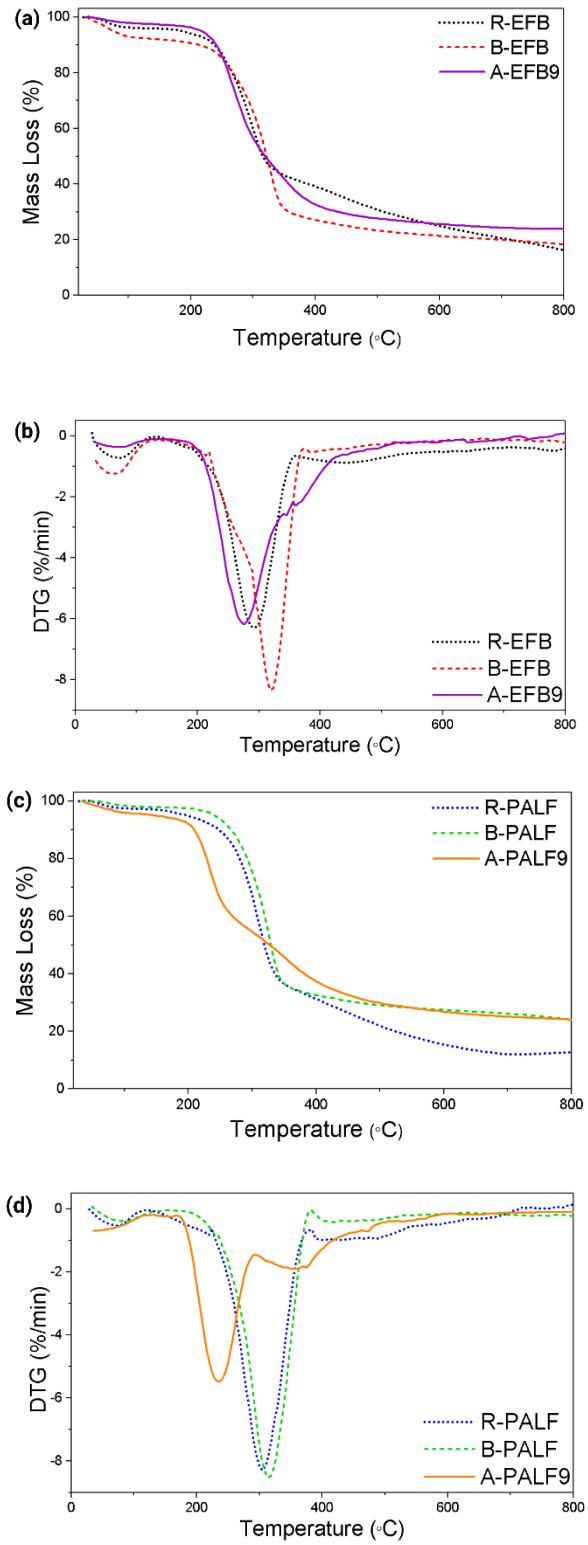

Figure 4 (a, c) TGA and (b, d) DTG curves for both EFB and PALF celluloses under different treatment conditions

Table 4 indicates that the T_{os} EFB and PALF CNCs were slightly lower than raw fibres. Nevertheless, the degradation temperature slowly increased with an extended reaction time. As observed in Figure 4, the dominant weight loss (more than 70%) in both fibre types happened up to 400 °C. The cellulose pyrolysis has likely contributed to the most significant weight loss in the respective temperature range. The decrease in the thermal stability of CNC might be caused by its small size. As depicted in TEM analysis, the double oxidative treatment had changed the fibre into nanometer-sized cellulose.

According to Sofla *et al.* [43], small-sized particles have a higher surface area, leading to early thermal degradation. Li *et al*. [42] also proposed faster heat transfer on samples with a larger surface area. In addition, the thermal degradation of PALF CNC was inferior compared to that of the EFB (Table 4). In fact, the DTG curve of PALF CNC also shifted to early degradation temperatures. This incident could also be related to the existence of a higher percentage of carboxyl groups on the PALF cellulose surface. Larazza *et al.* [45] found that a greater degree of carboxylation improved the matrix-cellulose interface, but it adversely affected thermal stability. After 400 °C, a slow decomposition rate continued and resulted in different residual weight percentages at 800 °C. Although, the presence of carboxylic groups induces earlier decomposition, it offers some advantages to the CNC, by slowing the solid residue charring process [35]. As a result, the char residue of CNCs is higher than raw fibres, as shown in Table 4.

Table 4 TGA results for EFB and PALF and their CNCs

Samples	T_{os} (°C)	T_{max}(°C)	Mass at 800 °C (%)
R-EFB	228.88	309.05	16.25
B-EFB	238.44	353.44	28.19
A-EFB9	235.06	435.06	23.80
R-PALF	239.03	339.03	12.78
B-PALF	248.07	338.07	23.95
A-PALF9	204.89	409.80	24.11

*T_{OS}=Onset degradation temperature;
T_{max}=Maximum degradation temperature*

4.0 CONCLUSION

The present study shows that CNC from EFB and PALF were successfully prepared using the double oxidative treatment (bleaching and APS oxidation). Pre-treatment with bleaching enables the subsequent production of nanocellulose with APS treatment to be carried out in a lesser time of 9 hrs. FTIR analysis confirmed the progressive removal of non-cellulosic components during both chemical processes that enhanced the XRD crystallinity indices (CrI). XRD results also demonstrated that the CrI values for EFB were higher than those of PALF, but with a lower yield. The TEM analysis reveals that the obtained EFB and PALF CNC have distinct morphological characteristics; spherical shape and rod-like shape, respectively. The lower thermal stability of extracted CNC compared to the raw fibre was attributed to its smaller size (in nanometres), high surface area and high aspect ratio. The yield percentage of Minor differences in the CNC features regarding EFB and

PALF indicate that fibre type is a determining factor for cellulose extraction. The adopted approach also proved feasible for preparing nanocellulose from various biomass wastes.

Acknowledgement

The authors would like to express their gratitude to the Ministry of Higher Education Malaysia (MOHE) for the financial aid which facilitated the success of this project under the Financial Research Grant Scheme (Grant No: FRGS/1/2019/TK05/UIAM/02/8), and the International Islamic University Malaysia (IIUM).

References

[1] Xie, H., Du, H., Yang, X. and Si, C. 2018. Recent Strategies in Preparation of Cellulose Nanocrystals and Cellulose Nanofibrils Derived from Raw Cellulose Materials. *International Journal of Polymer Science*. 2018: 7923068. DOI: https://doi.org/10.1155/2018/7923068.

[2] Yang, H., Zhang, Y., Kato, R. and Rowan, S. J. 2019. Preparation of Cellulose Nanofibers from Miscanthus X. Giganteus by Ammonium Persulfate Oxidation. *Carbohydrate Polymers*. 212: 30-39. DOI: https://doi.org/10.1016/j.carbpol.2019.02.008.

[3] Li, Y., Liu, X., Nie, X., Yang, W., Wang, Y., Yu, R. and Shui, J. 2019. Multifunctional Organic-inorganic Hybrid Aerogel for Self-cleaning, Heat-insulating, and Highly Efficient Microwave Absorbing Material. *Advanced Functional Materials*. 29: 1807624 DOI: https://doi.org/10.1002/adfm.201807624.

[4] Thai, Q. B., Nguyen, S. T., Ho, D. K., Tran, T. D., Huynh, D. M., Do, N. H. N., Luu, T. P., Le, P. K., Le, D. K., Phan-Thien, N. and Duong, H. M. 2020. Cellulose-based Aerogels from Sugarcane Bagasse for Oil Spill-cleaning and Heat Insulation Applications, *Carbohydrate Polymers*. 228: 115365. DOI: https://doi.org/10.1016/j.carbpol.2019.115365.

[5] Chen, W., Yu, H., Lee, S. Y., Wei, T., Li, J. and Fan, Z. 2018. Nanocellulose: A Promising Nanomaterial for Advanced Electrochemical Energy Storage. *Chemical Society Reviews*. 47: 2837-2872.

[6] Shao, L., Cao, Y., Li, Z., Hu, W., Li, S. and Lu, L. 2018. Dual Responsive Aerogel Made from Thermo/Ph Sensitive Graft Copolymer Alginate-G-P(NIPAM-Co-NHMAM) for Drug-Controlled Release. International *Journal Biological Macromolecules*. 114: 1338-1344. DOI: https://doi.org/10.1016/j.ijbiomac.2018.03.166.

[7] Lazim, N. H. and Samat, N. 2019. The Influence of Irradiated Recycled Polypropylene Compatibilizer on the Impact Fracture Behavior of Recycled Polypropylene / Microcrystalline Cellulose Composites. *Polymer Composites*. 41: E24-E34. DOI: https://doi.org/10.1002/pc.24430.

[8] Awanis, J., Anis Sofia, S. and Samat, N. 2012. Effect of Coupling Agent on Mechanical Properties of Composite from Microcrystalline Cellulose and Recycled Polypropylene. *Advanced Material Research*. 576: 390-393.

[9] Long, L. Y., Wang, Y-X. and Wang, Y-Z. 2018. Cellulose Aerogels: Synthesis, Applications, and Prospects. *Polymers*. 10(6): 623. DOI: https://doi.org/10.3390/polym10060623.

[10] Ritchie, H. and Roser, M. 2021. Palm Oil - Our World in Data. https://ourworldindata.org/palm-oil.

[11] Shahbandeh, M. 2019. Leading Countries in Pineapple Production Worldwide. https://www.statista.com/statistics/298517/global-pineapple-production-by-leading-countries.

[12] De France, K., Hoare, T. and Cranston, E. D. 2017. Review of Hydrogels and Aerogels Containing Nanocellulose. *Chemistry of Materials*. 29(11): 4609-4631. DOI: https://doi.org/10.1021/acs.chemmater.7b00531.

[13] Rohaizu, R. and Wanrosli, W. D. 2017. Sono-assisted TEMPO Oxidation of Oil Palm Lignocellulosic Biomass for Isolation of Nanocrystalline Cellulose. *Ultrasonics Sonochemistry*. 34: 631-639.

[14] Mawanto, Maulana M. I., Febrianto, F., Wistara, N. J., Nikmatin, S., Masruchin, N., Zaini, L. H., Lee, S. H. and Kim, N. H. 2021. Effect of Oxidation Time on the Properties of Cellulose Nanocrystals Prepared from Balsa and Kapok Fibers Using Ammonium Persulfate. *Polymers*. 13: 1894. DOI: https://doi.org/10.3390/polym13111894.

[15] Gabriel, T., Belete, A., Hause, G., Neubert, N. H. H. and Gebre-Mariam, T. 2021 Isolation and Characterization of Cellulose Nanocrystals from Different Lignocellulosic Residues: A Comparative Study. *Journal of Polymers and the Environment*. 29: 2964-2977. DOI: https://doi.org/10.1007/s10924-021-02089-3.

[16] Xu, X., Liu, F., Jiang, L., Zhu, J. Y., Haagenson, D., and Wiesenborn, D. P. 2013. Cellulose Nanocrystals vs. Cellulose Nanofibrils: A Comparative Study on Their Microstructures and Effects as Polymer Reinforcing Agents. *ACS Appl. Mater. Interfaces*. 5(8): 2999-3009.

[17] Niu, F., Li, M., Huang, Q., Zhang, X., Pan, W., Yang, J. and Li, J. 2017. The Characteristic and Dispersion Stability of Nanocellulose Produced by Mixed Acid Hydrolysis and Ultrasonic Assistance. *Carbohydrate Polymers*. 165: 197-204. DOI: https://doi.org/10.1016/j.carbpol.2017.02.048.

[18] Jiang, F. and Hsieh, Y. L. 2013. Chemically and Mechanically Isolated Nanocellulose and Their Self-Assembled Structures. *Carbohydrate Polymers*. 95: 32-40. DOI: https://doi.org/10.1016/j.carbpol.2013.02.022.

[19] Gan, P. G., Sam, S. T., Abdullah, M. F., Omar, M. F. and Tan, L. S. 2020. An Alkaline Deep Eutectic Solvent Based on Potassium Carbonate and Glycerol as Pretreatment for the Isolation of Cellulose Nanocrystals from Empty Fruit Bunch. *BioResources*. 15: 1154-1170.

[20] Bashar, M. M., Zhu, H., Yamamoto, S. and Mitsuishi, M. 2019. Highly Carboxylated and Crystalline Cellulose Nanocrystals from Jute Fiber by Facile Ammonium Persulfate Oxidation. *Cellulose*. 26: 3671-3684. DOI: https://doi.org/10.1007/s10570-019-02363-7.

[21] Leung, A. C. W., Hrapovic, S., Lam, E., Liu, Y., Male, K. B., Khaled, A. M. and Luong, J. H. T. 2011. Characteristics and Properties of Carboxylated Cellulose Nanocrystals Prepared from a Novel One-Step Procedure. *Small*. 7(3): 302-305.

[22] Haniffa, M. A. C. M., Ching, Y. C., Chuah, C. H., Kuan, Y. C., Nik Nazri, Abdullah, L. C., and Nai-Shang, L. 2017. Effect of TEMPO-Oxidization and Rapid Cooling on Thermo-structural Properties of Nanocellulose. *Carbohydrate Polymers*. 173: 91-99. DOI: https://doi.org/10.1016/j.carbpol.2017.05.084.

[23] Oun, A. A. and Jong-Whan, R. 2017. Characterization of Carboxymethyl Cellulose-Based Nanocomposite Films Reinforced with Oxidized Nanocellulose Isolated using Ammonium Persulfate Method. *Carbohydrate Polymers*. 174: 484-492. DOI: http://doi.org/10.1016/j.carbpol.2017.06.121,

[24] Mascheroni, E., Rampazzo, R., Ortenzi, M. A., Piva, G., Bonetti, S. and Piergiovanni, L. 2016. Comparison of Cellulose Nanocrystals Obtained by Sulfuric Acid Hydrolysis and Ammonium Persulfate, to be Used as Coating on Flexible Food-packaging Materials. *Cellulose*. 23: 779-793. DOI: http://doi.org/10.1007/s10570-015-0853-2

[25] Cheng, M., Qin, Z., Liu, Y., Qin, Y., Li, T., Chen, L. and Zhu, M. 2014. Efficient Extraction of Carboxylated Spherical Cellulose Nanocrystals with Narrow Distribution through Hydrolysis of Lyocell Fibers by Using Ammonium Persulfate as an Oxidant. *Journal of Materials Chemistry A*. 2(1): 251-258.

[26] Yang, H., Zhang, Y., Kato, R. and Rowan, S. J. 2019. Preparation of Cellulose Nanofibers from Miscanthus X.

Giganteus By Ammonium Persulfate Oxidation. *Carbohydrate Polymers*. 212: 30-39.
DOI: https://doi.org/10.1016/j.carbpol.2019.02.008.

[27] Goh, K. Y., Ching, Y. C., Chuah, C. H., Luqman, C. A. and Liou, N. S. 2016. Individualization of Microfibrillated Celluloses from Oil Palm Empty Fruit Bunch: Comparative Studies between Acid Hydrolysis and Ammonium Persulfate Oxidation. *Cellulose*. 23(1): 379-390.
DOI: https://doi.org/10.1007/s10570-015-0812-y

[28] Filipova, I., Fridrihsone, V., Cabulis, U., and Berzins, A. 2018. Synthesis of Nanofibrillated Cellulose by Combined Ammonium Persulphate Treatment with Ultrasound and Mechanical Processing. *Nanomaterials*. 8(640): 1-11.
DOI: https://doi.org/10.1007/s10570-020-03089-7.

[29] Du, C., Liu, M., Li, B., Li, H., Meng Q. and Zhan, H. 2016. Cellulose Nanocrystals Prepared by Persulfate One-Step Oxidation of Bleached Bagasse Pulp. *Bioresources*. 11(2): 4017-4024.

[30] Zhang, H., Chen, Y., Wang, S., Ma, L., Yu, Y., Dai, H. and Zhang, Y. 2020. Extraction and Comparison of Cellulose Nanocrystal from Lemon (Citrus Limon) Seeds Using Sulfuric Acid Hydrolysis and Oxidation Methods. *Carbohydrate Polymers*. 238: 116180.
DOI: https://doi.org/10.1016/j.carbpol.2020.116180.

[31] Dai, H., Ou, S., Huang, Y. and Huang, H. 2018. Utilization of Pineapple Peel for Production of Nanocellulose and Film Application. *Cellulose*. 25: 1743-1756.
DOI: http://doi.org/10.11113/jt.v79.9987.

[32] Fareez, I. A., Ain, I., Hanif, W. Y., Amira, M. R., Ainil, H. J. and Fauziah, A. A. 2018. Characteristics of Cellulose Extracted from Josapine Pineapple Leaf, Fibre After Alkali Treatment Followed by Extensive Bleaching. *Cellulose*. 25: 4407-4421.
DOI: http://doi.org/10.1007/s10570-018-1878-0.

[33] Ching, Y. C. and Ng, T. S. 2014. Effect of Preparation Conditions on Cellulose from Oil Palm Empty Fruit Bunch Fiber. *BioResources.* 9(4): 6373-6385.

[34] Zhang, K., Sun, P., Liu, H., Shang, S., Song, J., and Wang, D. 2016. Extraction and Comparison of Carboxylated Cellulose Nanocrystals from Bleached Sugarcane Bagasse Pulp using Two Different Oxidation Methods. *Carbohydrate Polymers.* 138: 237-243.

[35] Hu, Y., Tang, L., Lu, Q., Wang, S., Chen, X. and Huang, B. 2014. Preparation of Cellulose Nanocrystals and Carboxylated Cellulose Nanocrystals from Borer Powder of Bamboo. *Cellulose*. 21(3): 1611-1618.
DOI: https://doi.org/10.1007/s10570-014-0236-0.

[36] Azrina, Z. A. Z., Beg, M. D. H., Rosli, M. Y., Ramli, R., Junadi, N. and Alam, M. A. K. M. 2017. Spherical Nanocrystalline Cellulose (NCC) from Oil Palm Empty Fruit Bunch Pulp Via Ultrasound Assisted Hydrolysis. *Carbohydrate Polymers*. 162: 115-120.
DOI: https:// doi.org/10.1016/j.carbpol.2017.01.035.

[37] Burhani, D. and Septevani, A. A. 2018. Isolation of Nanocellulose from Oil Palm Empty Fruit Bunches Using Strong Acid Hydrolysis. *AIP Conference Proceedings*. 2024: 020005.
DOI: https://doi.org/10.1063/1.5064291.

[38] Deepa, B., Abraham, E., Cordeiro, N., Mozetic, M., Mathew, A. P., Oksman, K., Faria, M., Thomas, S. and Pothan, L. A. 2015. Utilization of Various Lignocellulosic Biomass for the Production of Nanocellulose: A Comparative Study. *Cellulose*. 22: 1075-1090.
DOI: https://doi.org/10.1007/s10570-015-0554-x.

[39] Ravindrana, L., Sreekala, M. S. and Thomas, S. 2019. Novel Processing Parameters for the Extraction of Cellulose Nanofibres (CNF) from Environmentally Benign Pineapple Leaf Fibres (PALF): Structure-Property Relationships. *International Journal of Biological Macromolecules*. 131: 858-870.
DOI: https://doi.org/10.1016/j.ijbiomac.2019.03.134.

[40] Mahardika, M., Abral, H., Kasim, A., Arief, S. and Asrofi, M. 2018. Production of Nanocellulose from Pineapple Leaf, Fibers Via High-Shear Homogenization and Ultrasonication. *Fibers*. 6(2): 28.
DOI: https://doi.org/10.3390/fib6020028.

[41] Hall, M., Bansal, P., Lee J. H., Realff, M. J. and Bommarius, A. S. 2010. Cellulose Crystallinity – A Key Predictor of the Enzymatic Hydrolysis Rate. *The FEBS Journal*. 277: 1571-1582.

[42] Grierer, J. 1986. Chemistry of Delignification. *Wood Science and Technology*. 20(1): 1-33.

[43] Sofla, M. R. K., Brown, R. J., Tsuzuki, T. and Rainey, T. J. 2016. A Comparison of Cellulose Nanocrystal and Cellulose Nanofibers Extracted from Bagasse Using Acid and Ball Milling Methods. *Advances in Natural Science: Nanoscience and Nanotechnology*. 7: 035004.

[44] Li, Y., Liu, X., Nie, X., Yang, W., Wang, Y., Yu, R. and Shui, J. 2019. Multifunctional Organic-inorganic Hybrid Aerogel for Self-cleaning, Heat-Insulating, and Highly Efficient Microwave Absorbing Material. *Advanced Functional Materials*. 29(10): 1807624.
DOI: https://doi.org/10.1002/adfm.201807624.

[45] Larraza, I., Vadillo, J., Santamaria-Echart, A., Tejado, A., Azpeitia, M., Vesga, E., Orue, A., Saralegi, A., Arbelaiz, A. and Eceiza, A. 2020. The Effect of the Carboxylation Degree on Cellulose Nanofibers and Waterborne Polyurethane/Cellulose Nanofiber Nanocomposites Properties. *Polymer Degradation and Stability*. 173: 109084.
DOI: https://doi.org/10.1016/j.polymdegradstab.2020.109084.